Barker, P.F., Camerlenghi, A., Acton, G.D., and Ramsay, A.T.S. (Eds.)
Proceedings of the Ocean Drilling Program, Scientific Results Volume 178

10. Identification of the Glacial Signal from the Antarctic Peninsula since 3.0 Ma at Site 1101 in a Continental Rise Sediment Drift[1]

Ellen A. Cowan[2]

ABSTRACT

Sediment drifts on the continental rise west of the Antarctic Peninsula received fine-grained sediment and ice-rafted debris (IRD) directly from the continental shelf and thus indirectly record the history of West Antarctic glaciation. Site 1101 contains a 218-m-thick, nearly continuous section extending from the late Pliocene to the Holocene. To assess the presence of calving glaciers at sea level in the Antarctic Peninsula region, the mass accumulation rate (MAR) of IRD was calculated using the weight percent terrigenous sand fraction (250 µm to 2 mm). IRD MAR is cyclic throughout, with small peaks alternating with periods of low or no IRD. Many cycles have a sawtooth pattern that increases gradually to the peak then abruptly decreases to zero. This pattern is consistent with rapid disintegration of ice streams and release of icebergs from the continental shelf. Three unusually large peaks (three to five times the size of other peaks) occurred at approximately 2.8, 1.9, and 0.88 Ma and indicate periods of intense ice rafting.

Lithofacies were described in detail using X-radiographs and core descriptions for the interval from 1.34 to 0.54 Ma. Glacial units are represented by thickly laminated mud deposited by distal turbidites and meltwater plumes. Less commonly, thinly laminated sediment formed by contour currents and diamicton by intense ice rafting. Interglacials are represented by foraminifer-bearing mud with IRD. Ice rafting appears to have increased in the later part of the glacial period and remained high in the interglacial period.

[1]Cowan, E.A., 2001. Identification of the glacial signal from the Antarctic Peninsula since 3.0 Ma at Site 1011 in a continental rise sediment drift. *In* Barker, P.F., Camerlenghi, A., Acton, G.D., and Ramsay, A.T.S. (Eds.), *Proc. ODP, Sci. Results,* 178, 1–22 [Online]. Available from World Wide Web: <http://www-odp.tamu.edu/publications/178_SR/VOLUME/CHAPTERS/SR178_10.PDF>. [Cited YYYY-MM-DD]
[2]Department of Geology, Appalachian State University, PO Box 32067, Boone NC 28608, USA.
cowanea@appstate.edu

Initial receipt: 8 August 2000
Acceptance: 5 April 2001
Web publication: 24 July 2001
Ms 178SR-206

INTRODUCTION

Sediment mounds on the continental rise west of the Antarctic Peninsula receive fine-grained sediment and ice-rafted debris (IRD) directly from the continent, thus indirectly recording the history of West Antarctic glaciation. The objective of this study is to interpret this record at Site 1101, which contains a nearly continuous sedimentary section extending from the late Pliocene to Holocene. The terrigenous lithofacies at this site are controlled by variable sedimentary processes and rates that are determined by the proximity of the glacial source to the continental shelf edge. IRD is identified as the coarse-grained component ranging from >250 µm to pebbles. The presence of IRD indicates periods when glaciers extended to sea level and distributed sediment by icebergs.

Site 1101 is located distally within Drift 4 on the continental rise ~94 km from the shelf edge (Fig. F1) (Rebesco et al., 1997, 1998). This asymmetrically shaped sediment drift is flanked on both sides by turbidite channels that convey sediment originating from the continental shelf to the Palmer deep-sea fan. On the continental shelf, troughs were carved by thick, 100-km-wide fast-flowing ice streams that were grounded at the shelf edge during glacial maxima (Pope and Anderson, 1992; Bart and Anderson, 1995; Pudsey et al., 1994). The trough inshore of Drift 4 is flanked by two sediment lobes (Lobes 2 and 3 in Fig. F1), which were deposited under thin, slowly moving ice (Rebesco et al., 1998). Significant volumes of coarse-grained, unsorted sediment were moved through the troughs and were deposited on the continental slope when the ice streams were near the shelf edge. Failure of this unstable sediment and meltwater plumes discharging from beneath ice streams resulted in high sediment accumulation rates on the drifts. Once the ice sheet became unstable because of rising sea level and a negative glacial mass balance, rapid disintegration by iceberg calving is predicted because of the few pinning points on the continental shelf beyond the northwest coastline of the large islands (Larter and Cunningham, 1993). During interglacials, this terrigenous sediment supply to the continental rise is cut off because (1) the shelf is too deep to be reworked by wind-generated currents or storms and (2) the shelf deepens toward the continent.

The sediments at Site 1101 were divided into three lithostratigraphic units (see Barker, Camerlenghi, Acton et al., 1999, for core photographs and descriptions). Unit I (0–53.3 meters below sea floor [mbsf]) and Unit II (53.3–142.7 mbsf) are composed of biogenic-bearing homogeneous muds alternating with predominantly laminated terrigenous muds that are interpreted to have been deposited during interglacial and glacial periods, respectively. A major difference between Units I and II is the composition of the biogenic component. Unit I contains diatom-bearing interglacial layers, whereas Unit II contains foraminifer-bearing layers. Unit III (142.7–217.7 mbsf) lacks the regular alternation of biogenic and terrigenous intervals observed above. However, it shows a strong glacial influence in the deposition of ice-rafted diamicton.

This study uses the IRD record from the Antarctic Peninsula as one aspect of the glacial signal since 3.0 Ma. IRD deposition is controlled by many factors, including oceanic conditions, ice thermal regime, and bedrock erodibility, as well as the ice volume on the continent (Denton et al., 1991). This study follows an approach similar to that used by

F1. Location map of Site 1101 on Drift 4, p. 17.

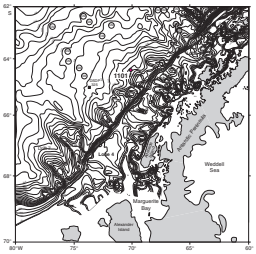

Grobe and Mackensen (1992) and heeds Anderson's (1999) recent warning that detailed sedimentologic investigations are necessary to interpret the IRD flux with respect to depositional processes and sedimentation rates that vary greatly. Site 1101 provides an opportunity to interpret the IRD mass accumulation rate (MAR) with respect to other sedimentary processes, because its location near the continent resulted in high sedimentation rates and a high-resolution record with an identifiable glacial–interglacial cyclicity.

MATERIALS AND METHODS

Samples for IRD analysis were taken at regularly spaced intervals throughout the 218-m sedimentary section at Site 1101. Although the fine-grained sediments at this site do not contain any visible hiatuses, the site was cored only once and therefore it is not possible to determine if there are any gaps between cores. The depth spacing between samples, average linear sedimentation rates, and resulting temporal resolution of samples are summarized in Table T1. The sedimentation rates used to calculate ages are based on shipboard paleomagnetic and biostratigraphic datums (Barker, Camerlenghi, Acton, et al., 1999). The high sedimentation rates and relatively close sample spacing result in a temporal resolution that is high enough to identify the IRD flux within both glacial and interglacial intervals. However, magnetostratigraphy does not provide data necessary to estimate variations in sediment accumulation rates between glacial and interglacial periods. Based on analogy with modern glacimarine environments and the amount of bioturbation in the sediment record, sediment appears to have accumulated much more rapidly in glacial intervals than in interglacials. Variability in sediment delivery rates is also expected during glacial periods. For example, Pudsey (2000) calculated sedimentation rates using gravity cores from drift sites and found that they ranged from 1.8 to 13.5 cm/ka during glacial stages.

T1. Summary of depth ranges sampled, p. 22.

Lithofacies analysis utilized shipboard core descriptions (Barker, Camerlenghi, Acton, et al., 1999) and X-radiography of U-channel samples that were collected for shore-based paleomagnetic studies.

IRD MAR Calculation

Calculation of the IRD MAR follows the method developed by Krissek (1995) for Ocean Drilling Program (ODP) cores from the North Pacific. IRD abundance was determined from the 250-µm to 2-mm sand fraction, which was separated by wet sieving after air drying, rinsing with distilled water to remove salts, and ultrasonic vibration. The 250-µm to 2-mm fraction was dried, weighed, and the abundance of the coarse sand fraction (in weight percent) was calculated. The sand was then examined with a binocular microscope to estimate the volume of terrigenous ice-rafted sediment (in volume percent) in order to exclude biogenic components, volcanic ash, and manganese micronodules, which usually do not have an ice-rafted origin. Following Krissek (1995), the IRD MAR (in grams per square centimeter per thousand years) was calculated as

$$\text{IRD MAR} = \text{CS\%} \times \text{IRD\%} \times \text{DBD} \times \text{LSR},$$

where CS% = the coarse sand abundance (multiplied as a decimal), IRD% = the IRD abundance in the coarse sand fraction (as a volume ratio), DBD = the dry bulk density of the whole sediment sample (in grams per cubic centimeter) determined from the measurement of dry bulk density on the discrete sample taken closest to the depth sampled for IRD (see "Physical Properties" in the "Explanatory Notes" chapter in Barker, Camerlenghi, Acton, et al., 1999), and LSR = the interval average linear sedimentation rate (in centimeters per thousand years).

X-Radiography

The U-channel samples provided 2 cm × 2 cm × 150 cm strips from the center of the working half of most cores to 124 mbsf for X-radiography. A few cores were not sampled because they were disturbed during coring. Although the width is narrow, U-channel samples are of uniform thickness and are continuous through each core, making them ideal for X-radiography. Three U-channel samples were X-rayed per sheet of Kodak Industrex-M film using a portable MinXray 803 with settings of 80 kV and 20 mA. The 150-cm-long U-channel samples were exposed for 26 s in 40-cm-long overlapping sections. Each film was contact printed and spliced together to make a true-scale image of the U-channel sample. These X-radiographs were used to describe sedimentary structures and to identify lithofacies. Clasts >2 mm were counted at 1-cm spacing following the method described by Grobe (1987) to provide more continuous data than the IRD MAR method. The volume of sediment represented on each X-radiograph is 2 cm (width) × 2 cm (thickness) × 1 cm (counting interval) = 4 cm^3.

RESULTS

IRD Mass Accumulation Rates

IRD abundance (in weight percent) and MAR are presented in the "Appendix," p. 12, and Figure F2. IRD abundance is cyclic throughout, with small peaks alternating with periods of low or no IRD. IRD abundance fluctuates within a range of 0–2.0 wt%, except within three intervals: two peaks between 195.7 and 204.3 mbsf, 128.8 mbsf, and 60.7–62.2 mbsf (Fig. F2A). These peaks range from 2.5 to 3.7 wt% IRD, and the first and third intervals coincide with 20- to 50-cm-thick diamicton beds. These diamicton beds show characteristics attributed to deposition from ice rafting that include gradational contacts, weak stratification, and random pebble orientation (Cowan et al., 1997). The MAR profile has an appearance similar to the IRD abundance with three unusually large peaks (three to five times the size of the other peaks) at ~2.8 (Fig. F2B, interval a), 1.9 (Fig. F2B, interval b) and 0.88 Ma (Fig. F2B, interval c). Between these large peaks, there are many smaller frequency cycles produced by peaks in MAR that alternate with low or no IRD. One prolonged period of low MAR occurs from 2.12 to 1.98 Ma. Many cycles have a sawtooth pattern that increases gradually upsection to the peak MAR then abruptly decreases to zero. An example of one such prominent cycle occurs from 0.65 to 0.55 Ma. Visually, the IRD MAR record at Site 1101 is divided into three intervals of ~1-Ma duration (Fig. F2B). In intervals a–b and b–c (Fig. F2B), the general trend is for the magnitude of the highest MAR peaks within a cycle to decrease through the interval then abruptly increase at the prominent peak. In

F2. Abundance and accumulation rate of coarse sand-sized IRD, p. 18.

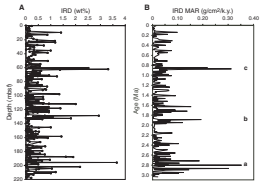

the upper interval (above c) (Fig. F2B) this MAR trend is reversed, with the peaks gradually increasing until an abrupt decrease at 0.1 Ma. The frequency of peaks in the upper interval is also greater than in a–b and b–c (Fig. F2B).

Lithofacies Analysis

Within the interval from 95 to 38 mbsf (Sections 178-1101A-11H-7 to 6H-1), sediments were categorized by lithofacies using core descriptions and X-radiographs (Fig. F3). This interval, from 1.37 to 0.54 Ma, was chosen for detailed study because it contains the Jaramillo Subchron and the Brunhes/Matuyama boundary. It has well-defined alternations between foraminifer-bearing homogeneous mud representative of interglacials and terrigenous laminated or homogeneous mud without foraminifers deposited during glacial periods (Barker, Camerlenghi, Acton, et al., 1999). The contrast in magnetic susceptibility (MS) between the carbonate-bearing interglacials and the low-carbonate terrigenous glacial intervals has produced a well-defined cyclicity throughout (Fig. F3). Most sections were X-rayed, and this allowed for further characterization of sedimentary structures and a count of IRD >2 mm in 1-cm increments (Fig. F3). The prominent peak c (Fig. F2B) occurs at 0.88 Ma (62.2–60.7 mbsf), and therefore, the timing of this and other peaks in IRD with regard to glacial–interglacial cyclicity can be investigated.

F3. Lithofacies description, Site 1101, p. 19.

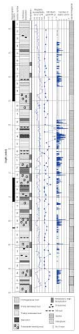

F4. X-radiographs of laminated mud, p. 20.

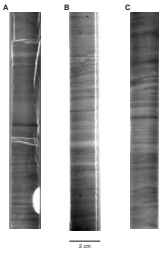

DESCRIPTION AND INTERPRETATION OF LITHOFACIES

Thickly laminated mud lithofacies is present commonly within the studied interval (Fig. F3). Parallel silt laminae are >2 mm thick and have sharp lower contacts and grade upward into mud. On X-radiographs, they appear as medium-density fuzzy laminations with low-density interlaminae (Fig. F4A, F4B). The MS signature has high-frequency peaks, and thicker silt laminae correspond to peak MS values. Bioturbation is slight, with burrowing parallel to laminae or absent. IRD is present as isolated pebbles or as weak stratification (Fig. F4B). This lithofacies was deposited during glacial periods by distal low-density turbidity currents, probably generated by sediment failure along the continental slope (McGinnis et al., 1997; Barker et al., 1999) or by rapid hemipelagic sedimentation from meltwater plumes originating at glacier margins near the shelf edge (Pudsey, 2000). This lithofacies is punctuated by intervals of intense iceberg rafting.

The thinly laminated mud lithofacies has 1- to 2-mm-thick parallel to wavy laminae that appear color banded or variegated on the split core surface. This lithofacies has a distinctive appearance on X-radiographs: a strong contrast between thin silt and mud laminae (Fig. F4C). This is interpreted to visually indicate sharp contacts between the silt and mud laminae. IRD is low and variable within this lithofacies. The thinly laminated lithofacies appears significantly different from other laminated lithofacies on X-radiographs and on the split core surface. The sharp contacts and wavy laminae may result from reworking and winnowing of fine-grained turbidites by currents. These siliciclastic-dominated laminae have several characteristics in common with glacigenic contourites (Stoker et al., 1998). However, the origin of the thinly laminated lithofacies cannot be definitively determined without

further work because of the many similarities that exist between fine-grained turbidites and those that have been reworked by contour currents (Stow et al., 1998). However, these two lithofacies suggest that several processes may have operated on the Antarctic Peninsula continental rise during glacial periods. At present, contour currents are steady but have too low a velocity to erode drift sediment (Camerlenghi et al., 1997). Contour current strength may vary between glacial and interglacial periods, as has been suggested for the Weddell Sea by Grobe and Mackensen (1992).

Homogeneous mud appears as a low-density massive unit on X-radiographs with isolated IRD (Fig. F5A, F5B). Bioturbation may be high, resulting in complete reworking locally. This lithofacies is structureless, either as a result of rapid hemipelagic sedimentation from meltwater plumes or from infaunal activity when sedimentation rates were low. Icebergs were present, but rapid sedimentation could have reduced their overall impact within the record.

Diamicton occurs in 20- to 50-cm-thick beds that are massive or weakly stratified with clasts concentrated in bands and silt laminae (Figs. F3, F5C). The diamicton was deposited by intense iceberg rafting with possible contributions of mud from meltwater plumes. This lithofacies corresponds to the highest IRD MAR and pebble counts within the studied interval.

Foraminifer-bearing mud contains 10%–90% biogenic component and isolated IRD. X-radiographs are low density and show highly burrowed sediment with loss of primary structures (Fig. F5D). Foraminifers are rare near the Antarctic continent (Hodell and Venz, 1992) and at the other sites drilled during Leg 178 (Barker, Camerlenghi, Acton, et al., 1999). Their abundance in the interglacial periods at Site 1101 from 2.2 to 0.76 Ma suggests that conditions favorable for carbonate preservation occurred during these warmer periods (Pudsey, 2000) and not at other times. Slow sedimentation allowed high infaunal activity and bioturbation along with homogenization of IRD.

Features on the IRD MAR curve and >2-mm clast histogram generally correspond (Fig. F3). The highest values coincide with diamicton, which supports its origin by ice rafting. Thinly laminated mud has the lowest IRD MAR, and other lithofacies have variable IRD MAR.

F5. X-radiographs of homogeneous mud, diamicton, and foraminifer-bearing mud, p. 21.

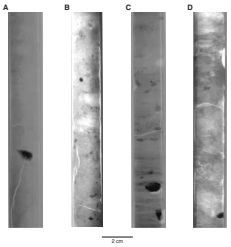

DISCUSSION

Interpretation of the IRD record and lithofacies in the paper suggests that there are eight glacial–interglacial cycles from 95 to 38 mbsf (1.37–0.54 Ma). This cyclicity is best recorded in the MS data because of the reduction in MS resulting from abundant carbonate in the interglacial periods (Fig. F3). From 95 to 67 mbsf, the interglacial and glacial intervals are thin relative to those above. Estimates of their duration using linear sedimentation rates indicate that these shorter-period cycles closely match the 41-k.y. cycles of orbital obliquity reported from marine cores in the Northern Hemisphere (Ruddiman et al., 1986; Ruddiman and Raymo, 1988). At ~1.01 Ma (72.4 mbsf), the glacial and interglacial intervals become thicker and the period lengthens to about 100 k.y. The timing of this transition is slightly earlier than that reported in the Northern Hemisphere (Ruddiman et al., 1986). At Site 1101, there is one long cycle prior to the Brunhes/Matuyama boundary; in the Northern Hemisphere, the 41-k.y. cycles continue up to 0.73 Ma.

Ice rafting follows a regular pattern throughout each glacial and interglacial period, with low or no IRD MAR in the first part of the glacial period and an increase after the midpoint with peaks >0.05 g/cm²/k.y. (Fig. F3). IRD MAR remains high within the interglacials and returns to low values prior to the start of the next glacial period. This pattern of ice rafting is consistent with rapid disintegration of ice streams and release of icebergs from the continental shelf. The IRD MAR peaks within the laminated fine-grained glacial units indicate very high rates of deposition, because the overall sedimentation rates were high during that time. During interglacials, the sedimentation rates were slower and allowed bioturbation, which would have concentrated the coarse-grained IRD within the biogenic-rich sediment. Significantly more debris was deposited in the peaks that occur around 0.88 Ma (between 62 and 60 mbsf) (Fig. F3) than at other times. This could result from extreme deglaciation of the Antarctic Peninsula that exposed debris-rich basal ice from glaciers draining inland fjords (cf. Anderson and Andrews, 1999). This rafting event occurs within the first 100-k.y. glacial interval following the transition from 41-k.y. to 100-k.y. cyclicity. Following this large peak, IRD MAR is lower, with only one peak >0.05 g/cm²/k.y. near the start of the next glacial. The previous pattern of ice rafting does not appear to be reestablished immediately after this large peak (Fig. F2B, interval c).

Lithofacies differ between glacial periods, but they are dominated by thickly laminated mud corresponding to deposition of either distal turbidites or plumites. Thinly laminated mud also occurs regularly within 41-k.y. glacial cycles below 69 mbsf and suggests that periods occurred when turbidity current activity was less and contour currents caused reworking. Within the 100-k.y. glacial intervals, thickly laminated mud alternates with homogeneous mud (Fig. F3). For example, above 53 mbsf there are six fining-upward packages of laminated mud grading into homogeneous mud that are easily observed on X-radiographs because of the density contrast between these two lithofacies. These may represent shorter-period cycles of glacier advance and retreat between proximal and distal locations on the shelf that did not occur previously.

IRD has been transported to the continental rise of the Antarctic Peninsula cyclically over the past 3 m.y. The first prominent peak at Site 1101 occurs at 2.8 Ma (interval a, Fig. F2B) prior to the onset of widespread Northern Hemisphere glaciation at ~2.4 Ma. Generally warm conditions are proposed from 2.9 to 2.48 Ma in the Southern Ocean (Ciesielski et al., 1982). Warmer glacial conditions are suggested at Site 1101 by the presence of diatom ooze within the laminated sediments and the highest sedimentation rates over the last 3.0 m.y. (Barker, Camerlenghi, Acton, et al., 1999). At Site 1101, intense ice rafting at ~2.8 Ma deposited diamicton beds associated with the large IRD MAR peak. However, IRD MAR is low at sites further away from the Antarctic continent, such as in the Argentine Basin (Bornhold, 1983), which may indicate fewer far-traveled icebergs because of more rapid iceberg melt closer to the continent. Warmer conditions on the Antarctic Peninsula may have resulted in warm-based glaciers that calved debris-laden icebergs such as those from Greenland, which would not travel as far as large tabular Antarctic icebergs.

Well-defined 41-k.y. cyclicity occurs at Site 1101 from 1.9 to 1.01 Ma. Prior to this time, IRD MAR peaks are of variable frequency and there are periods without peaks (i.e., 2.12–1.98 Ma). The onset of 41-k.y. cyclicity coincides with prominent peak b (Fig. F2B). The period between 2.6 and 1.67 Ma has been described as an intermediate stage in Antarc-

tic cryosphere development (Warnke et al., 1992). The largest peak at 0.88 Ma (Fig. F2B, interval a) is probably related to the mid-Pleistocene climate transition dated from 0.92 to 0.90 Ma in the Northern Hemisphere (Berger and Jansen, 1994). IRD is at a maximum during this time in the Southern Ocean (Ledbetter and Watkins, 1978) and the Argentine Basin (Bornhold, 1983). Bornhold (1983) attributed high IRD MAR from 0.90 to 0.65 Ma to changes in ocean circulation and more melting rather than increased Antarctic glaciation. Ice rafting from the Scandinavian ice sheet was also high in the Norwegian Sea during the mid-Pleistocene climate transition (Berger and Jansen, 1994). This bipolar connection between ice-rafting events may be related to modification of deep-ocean circulation. The North Atlantic Deep Water feeds the Antarctic Circumpolar Current, thus linking the North Atlantic with the Antarctic continent. Site 1101 is much closer to the continent than these other sites and therefore may be more influenced by the extent of deglaciation of the continent rather than ocean circulation. However, the widespread ice-rafting event at ~0.90 Ma may record changes on the continent and in ocean circulation so that icebergs could deposit debris both at proximal sites and in distant oceans. At Site 1101, prominent peak a (Fig. F2B) also coincides with the transition from 41-k.y. to 100-k.y cyclicity.

CONCLUSIONS

Sedimentation at Site 1101 since 3.0 Ma has recorded glacial–interglacial cyclicity at varying strengths and frequencies, including a strong 41-k.y. frequency from 2.2 to 1.0 Ma and 100-k.y. frequency after 1.0 Ma. During glacial periods, sediments are conveyed down the continental slope to the rise by turbidity currents and debris is rafted by icebergs. At Site 1101, glacial lithofacies most commonly consist of thickly laminated muds deposited from distal turbidites and meltwater plumes. Thinly laminated muds were deposited in short intervals dominated by contour currents. Diamictons were deposited at ~2.8 and 0.88 Ma, when ice rafting was intense. During interglacials, sediment was biogenic and dominated by foraminifers from 2.2 to 0.76 Ma. The sediment was nearly completely reworked by burrowing infauna, and few laminae are preserved. For this study, sediments were studied in greatest detail from 1.34 to 0.54 Ma. During this interval, ice rafting has a regular pattern, low during the first part of the glacial period, increasing in the later half, and remaining high in the following interglacial. This is consistent with rapid disintegration of ice streams and suggests that the contribution of IRD within the rapidly deposited laminated glacial units is very high. Sedimentation rates were probably slower in the bioturbated, homogeneous interglacials leading to greater concentration of IRD relative to the glacial units.

ACKNOWLEDGMENTS

This research was funded by a JOI-USSSP postcruise research grant. Lauren Hassler provided valuable laboratory assistance in processing samples for IRD MAR determination. Yohan Guyodo and Gary Acton skillfully collected the U-channel samples that were X-radiographed. Eugene Domack (Hamilton College) graciously loaned his portable X-ray machine for this project. Thanks to Fiona Taylor who provided valu-

able tips about its operation. Assistance in taking and processing the X-radiographs at Appalachian State University came from Keith Seramur, Marjorie McKinney, and Anthony Love. The manuscript was improved by critical reviews by Drs. D. Warnke and J. Smellie.

REFERENCES

Anderson, J.B., 1999. *Antarctic Marine Geology.* Cambridge (Cambridge University Press).

Anderson, J.B., and Andrews, J.T., 1999. Radiocarbon constraints on ice sheet advance and retreat in the Weddell Sea, Antarctica. *Geology,* 27:179–182.

Barker, P.F., Barrett, P.J., Cooper, A.K., and Huybrechts, P., 1999. Antarctic glacial history from numerical models and continental margin sediments. *Palaeogeogr., Palaeoclimatol., Palaeoecol.,* 150:247–267.

Barker, P.F., Camerlenghi, A., Acton, G.D., et al., 1999. *Proc. ODP, Init. Repts.,* 178 [CD-ROM]. Available from: Ocean Drilling Program, Texas A&M University, College Station, TX 77845-9547, U.S.A.

Bart, P.J., and Anderson, J.B., 1995. Seismic record of glacial events affecting the Pacific margin of the northwestern Antarctic Peninsula. *In* Cooper, A.K., Barker, P.F., and Brancolini, G. (Eds.), *Geology and Seismic Stratigraphy of the Antarctic Margin.* Am. Geophys. Union, Antarct. Res. Ser., 68:74–95.

Berger, W.H., and Jansen, E., 1994. Mid-Pleistocene climate shift: the Nansen connection. *In* Johannessen, O.M., Muensch, R.D., and Overland, J.E. (Eds.), *The Role of the Polar Oceans in Shaping the Global Environment.* Geophys. Monogr., Am. Geophys. Union, 85:295–311.

Bornhold, B.D., 1983. Ice-rafted debris in sediments from Leg 71, southwest Atlantic Ocean. *In* Ludwig, W.J., Krasheninnikov, V.A., et al., *Init. Repts. DSDP,* 71: Washington (U.S. Govt. Printing Office), 307–316.

Camerlenghi, A., Crise, A., Pudsey, C.J., Accerboni, E., Laterza, R., and Rebesco, M., 1997. Ten-month observation of the bottom current regime across a sediment drift of the Pacific margin of the Antarctic Peninsula. *Antarct. Sci.,* 9:426–433.

Ciesielski, P.F., Ledbetter, M.T., and Ellwood, B.B., 1982. The development of Antarctic glaciation and the Neogene paleoenvironment of the Maurice Ewing Bank. *Mar. Geol.,* 46:1–51.

Cowan, E.A., Cai, J., Powell, R.D., Clark, J.D., and Pitcher, J.N., 1997. Temperate glacimarine varves: an example from Disenchantment Bay, southern Alaska. *J. Sediment. Res.,* 67:536–549.

Denton, G.H., Prentice, M.L., and Burckle, L.H., 1991. Cainozoic history of the Antarctic ice sheet. *In* Tingey, R.J. (Ed.), *The Geology of Antarctica.* Oxford Monogr. Geol. Geophys., 17:365–433.

Grobe, H., 1987. A simple method for the determination of ice-rafted debris in sediment cores. *Polarforschung,* 57:123–126.

Grobe, H., and Mackensen, A., 1992. Late Quaternary climatic cycles as recorded in sediments from the Antarctic continental margin. *In* Kennett, J.P., and Warnke, D.A. (Eds.), *The Antarctic Paleoenvironment: A Perspective on Global Change* (Pt. 1). Am. Geophys. Union, Antarct. Res. Ser., 56:349–376.

Hodell, D.A., and Venz, K., 1992. Toward a high-resolution stable isotopic record of the Southern Ocean during the Pliocene-Pleistocene (4.8 to 0.8 Ma). *In* Kennett, J.P., Warnke, D.A. (Eds.), *The Antarctic Paleoenvironment: A Perspective on Global Change* (Pt. 1). Am. Geophys. Union, Antarct. Res. Ser., 56:265–310.

Krissek, L.A., 1995. Late Cenozoic ice-rafting records from Leg 145 sites in the North Pacific: late Miocene onset, late Pliocene intensification, and Pliocene–Pleistocene events. *In* Rea, D.K., Basov, I.A., Scholl, D.W., and Allan, J.F. (Eds.), *Proc. ODP, Sci. Results,* 145: College Station, TX (Ocean Drilling Program), 179–194.

Larter, R.D., and Cunningham, A.P., 1993. The depositional pattern and distribution of glacial-interglacial sequences on the Antarctic Peninsula Pacific Margin. *Mar. Geol.,* 109:203–219.

Ledbetter, M.T., and Watkins, N.D., 1978. Separation of primary ice-rafted debris from lag deposits, utilizing manganese micronodule accumulation rates in abyssal sediments of the Southern Ocean. *Geol. Soc. Am. Bull.,* 89:1619–1629.

McGinnis, J.P., Hayes, D.H., and Driscoll, N.W., 1997. Sedimentary processes across the continental rise of the southern Antarctic Peninsula. *Mar. Geol.,* 141:91–109.

Pope, P.G., and Anderson, J.B., 1992. Late Quaternary glacial history of the northern Antarctic Peninsula's western continental shelf: evidence from the marine record. *In* Elliot, D. H. (Ed.), *Contributions to Antarctic Research III.* Am. Geophys. Union, Antarct. Res. Ser., 57:63–91.

Pudsey, C.J., 2000. Sedimentation on the continental rise west of the Antarctic Peninsula over the last three glacial cycles. *Mar. Geol.,* 167:313–338.

Pudsey, C.J., Barker, P.F., and Larter, R.D., 1994. Ice sheet retreat from the Antarctic Peninsula shelf. *Cont. Shelf Res.,* 14:1647–1675.

Rebesco, M., Camerlenghi, A., and Zanolla, C., 1998. Bathymetry and morphogenesis of the continental margin west of the Antarctic Peninsula. *Terra Antart, 5:715–725.*

Rebesco, M., Larter, R.D., Barker, P.F., Camerlenghi, A., and Vanneste, L.E., 1997. The history of sedimentation on the continental rise west of the Antarctic Peninsula. *In* Barker, P.F., and Cooper, A.K. (Eds.), *Geology and Seismic Stratigraphy of the Antarctic Margin* (Pt. 2). Am. Geophys. Union, Antarctic Res. Ser., 71:29–50.

Ruddiman, W.F., Raymo, M., and McIntyre, A., 1986. Matuyama 41,000-year cycles: North Atlantic Ocean and Northern Hemisphere ice sheets. *Earth Planet. Sci. Lett.,* 80:117–129.

Ruddiman, W.F., and Raymo, M.E., 1988. Northern hemisphere climatic regimes during the past 3 Ma: possible tectonic connections. *Philos. Trans. R. Soc. London B,* 318:411–430.

Stoker, M.S., Akhurst, M.C., Howe, J.A., and Stow, D.A.V., 1998. Sediment drifts and contourites on the continental margin off northwest Britain. *Sediment. Geol.,* 115:33–51.

Stow, D.A.V., Faugères, J.C., Viana, A., and Gonthier, E., 1998. Fossil contourites: a critical review. *Sediment. Geol.,* 115:3–31.

Warnke, D.A., Allen, C.P., Muller, D.W., Hodell, D.A., and Brunner, C.A., 1992. Miocene-Pliocene Antarctic glacial evolution: a synthesis of ice-rafted debris, stable isotope, and planktonic foraminiferal indicators, ODP Leg 114. *In* Kennett, J.P., and Warnke, D.A. (Eds.), *The Antarctic Paleoenvironment: A Perspective on Global Change* (Pt. 1). Am. Geophys. Union, Antarct. Res. Ser., 56:311–325.

APPENDIX

Data Used to Calculate Mass Accumulation Rates of Coarse-Sand Ice-Rafted Debris at Site 1101

Core, section, interval (cm)	Depth (mbsf)	Calculated age (Ma)	Coarse sand weight (g)	IRD (volumetric ratio)	Dry bulk density (g/cm^3)	Linear sedimentation rate (cm/k.y.)	IRD (wt%)	IRD MAR (g/cm^2/k.y.)
178 1101A-								
1H-1, 50-52	0.50	0.007	0.02	0.90	0.762	7.061	0.239	0.013
1H-2, 50-52	2.00	0.028	0.01	1.00	0.762	7.061	0.123	0.007
1H-2, 125-127	2.75	0.039	0.00	1.00	0.762	7.061	0.019	0.001
1H-3, 50-52	3.50	0.050	0.00	1.00	0.813	7.061	0.023	0.001
1H-3, 125-127	4.25	0.060	0.02	1.00	0.813	7.061	0.140	0.008
1H-4, 50-52	5.00	0.071	0.00	1.00	0.813	7.061	0.017	0.001
1H-5, 50-52	6.50	0.092	0.00	1.00	0.878	7.061	0.069	0.004
1H-5, 125-127	7.25	0.103	0.02	1.00	0.878	7.061	0.161	0.010
1H-6, 50-52	8.00	0.113	0.02	0.50	0.878	7.061	0.077	0.005
2H-1, 125-127	9.95	0.141	0.11	0.90	0.987	7.061	1.420	0.099
2H-2, 50-52	10.70	0.152	0.01	1.00	0.878	7.061	0.068	0.004
2H-2, 125-127	11.45	0.162	0.02	1.00	0.987	7.061	0.152	0.011
2H-3, 50-52	12.20	0.173	0.01	1.00	0.987	7.061	0.057	0.004
2H-3, 125-127	12.95	0.183	0.11	1.00	0.987	7.061	0.866	0.060
2H-4, 50-52	13.70	0.194	0.00	1.00	0.987	7.061	0.036	0.003
2H-4, 125-127	14.45	0.205	0.00	1.00	0.987	7.061	0.029	0.002
2H-5, 50-52	15.20	0.215	0.02	1.00	0.987	7.061	0.237	0.016
2H-5, 125-127	15.95	0.226	0.00	1.00	0.987	7.061	0.008	0.001
2H-6, 125-127	17.45	0.247	0.01	1.00	0.987	7.061	0.051	0.004
3H-1, 50-52	18.70	0.265	0.02	1.00	0.873	7.061	0.308	0.019
3H-2, 50-52	20.20	0.286	0.04	1.00	0.873	7.061	0.449	0.028
3H-3, 50-52	21.70	0.307	0.10	1.00	0.955	7.061	1.170	0.079
3H-3, 125-127	22.45	0.318	0.02	1.00	0.955	7.061	0.125	0.008
3H-4, 50-52	23.20	0.329	0.02	0.90	0.87	7.061	0.208	0.013
3H-4, 125-127	23.95	0.339	0.10	1.00	0.87	7.061	1.181	0.073
3H-5, 49-51	24.69	0.350	0.01	1.00	0.87	7.061	0.053	0.003
3H-5, 125-127	25.45	0.360	0.01	1.00	0.87	7.061	0.051	0.003
3H-6, 50-52	26.20	0.371	0.00	1.00	1.028	7.061	0.012	0.001
3H-6, 125-127	26.95	0.382	0.01	1.00	1.028	7.061	0.056	0.004
3H-7, 40-42	27.60	0.391	0.04	1.00	1.028	7.061	0.454	0.033
4H-1, 50-51	28.20	0.399	0.06	1.00	1.028	7.061	0.722	0.052
4H-1, 125-126	28.95	0.410	0.00	1.00	1.028	7.061	0.031	0.002
4H-2, 50-51	29.70	0.421	0.03	1.00	1.028	7.061	0.191	0.014
4H-2, 125-126	30.45	0.431	0.05	1.00	1.028	7.061	0.324	0.024
4H-3, 50-51	31.20	0.442	0.04	1.00	1.045	7.061	0.336	0.025
4H-4, 50-51	32.70	0.463	0.02	1.00	1.028	7.061	0.153	0.011
4H-5, 50-51	34.20	0.484	0.00	1.00	1.072	7.061	0.010	0.001
4H-5, 125-126	34.95	0.495	0.03	1.00	1.072	7.061	0.326	0.025
4H-6, 50-51	35.70	0.506	0.10	1.00	1.072	7.061	0.998	0.076
4H-6, 125-126	36.45	0.516	0.05	1.00	1.072	7.061	0.459	0.035
4H-7, 50-51	37.20	0.527	0.01	1.00	0.963	7.061	0.153	0.010
4H-7, 83-84	37.53	0.532	0.06	1.00	0.963	7.061	0.461	0.031
5H-1, 44-45	37.64	0.533	0.03	1.00	0.963	7.061	0.389	0.026
5H-CC, 6-7	37.75	0.535	0.04	1.00	0.963	7.061	0.308	0.021
6H-1, 50-52	38.70	0.548	0.17	1.00	0.963	7.061	0.877	0.060
6H-1, 123-125	39.43	0.558	0.03	1.00	0.963	7.061	0.321	0.022
6H-2, 50-52	40.20	0.569	0.04	1.00	0.963	7.061	0.279	0.019
6H-3, 50-52	41.70	0.591	0.05	1.00	0.963	7.061	0.382	0.026
6H-4, 50-52	43.20	0.612	0.03	1.00	0.963	7.061	0.219	0.015
6H-5, 50-52	44.70	0.633	0.01	1.00	0.985	7.061	0.130	0.009
6H-6, 50-52	46.20	0.654	0.01	1.00	0.985	7.061	0.058	0.004
6H-7, 50-52	47.70	0.676	0.01	1.00	1.145	7.061	0.139	0.011
7H-1, 49-51	48.19	0.682	0.03	1.00	0.946	7.061	0.312	0.021
7H-1, 124-126	48.94	0.693	0.01	1.00	0.946	7.061	0.078	0.005
7H-2, 49-51	49.69	0.704	0.02	1.00	0.946	7.061	0.228	0.015
7H-2, 124-126	50.44	0.714	0.08	1.00	0.946	7.061	0.884	0.059
7H-3, 49-51	51.19	0.725	0.01	1.00	1.179	7.061	0.062	0.005
7H-3, 124-126	51.94	0.736	0.01	1.00	1.179	7.061	0.046	0.004
7H-4, 124-126	53.44	0.757	0.02	1.00	1.283	7.061	0.141	0.013
7H-5, 49-51	54.19	0.767	0.02	1.00	0.951	7.061	0.217	0.015
7H-5, 124-126	54.94	0.778	0.04	1.00	0.951	7.061	0.585	0.039
7H-6, 49-51	55.69	0.788	0.00	1.00	0.951	7.679	0.011	0.001
7H-6, 124-126	56.44	0.798	0.00	1.00	0.951	7.679	0.021	0.002

Appendix (continued).

Core, section, interval (cm)	Depth (mbsf)	Calculated age (Ma)	Coarse sand weight (g)	IRD (volumetric ratio)	Dry bulk density (g/cm^3)	Linear sedimentation rate (cm/k.y.)	IRD (wt%)	IRD MAR (g/cm^2/k.y.)
7H-7, 49-51	57.19	0.807	0.00	1.00	0.951	7.679	0.032	0.002
8H-1, 49-51	57.69	0.814	0.05	1.00	0.951	7.679	0.559	0.041
8H-1, 124-126	58.44	0.824	0.02	1.00	0.951	7.679	0.231	0.017
8H-2, 124-126	59.94	0.843	0.01	1.00	1.129	7.679	0.109	0.009
8H-3, 49-51	60.69	0.853	0.32	1.00	1.129	7.679	2.514	0.218
8H-3, 126-128	61.46	0.863	0.01	1.00	1.129	7.679	0.041	0.004
8H-4, 51-53	62.21	0.873	0.40	1.00	1.231	7.679	3.310	0.313
8H-4, 124-126	62.94	0.882	0.19	1.00	1.231	7.679	1.372	0.130
8H-5, 51-53	63.71	0.892	0.04	1.00	1.231	7.679	0.283	0.027
8H-5, 127-129	64.47	0.902	0.09	1.00	1.231	7.679	0.615	0.058
8H-6, 49-51	65.19	0.912	0.06	1.00	1.236	7.679	0.403	0.038
8H-6, 124-126	65.94	0.921	0.00	1.00	1.236	7.679	0.029	0.003
9H-1, 20-23	66.90	0.934	0.05	1.00	1.236	7.679	0.561	0.053
9H-1, 124-126	67.94	0.947	0.02	1.00	1.236	7.679	0.264	0.025
9H-2, 25-27	68.45	0.954	0.00	1.00	0.884	7.679	0.034	0.002
9H-2, 50-52	68.70	0.957	0.06	1.00	0.884	7.679	0.567	0.038
9H-2, 124-126	69.44	0.967	0.01	1.00	0.884	7.679	0.194	0.013
9H-3, 50-53	70.20	0.977	0.03	1.00	0.884	7.679	0.255	0.017
9H-3, 124-126	70.94	0.987	0.07	1.00	0.884	7.679	0.935	0.063
9H-4, 25-27	71.45	0.994	0.00	1.00	0.975	6.188	0.035	0.002
9H-4, 50-52	72.25	1.007	0.05	1.00	0.975	7.679	0.476	0.036
9H-4, 124-126	72.44	1.010	0.10	1.00	0.975	6.188	1.252	0.076
9H-5, 25-27	72.95	1.018	0.00	1.00	0.975	6.188	0.007	0.000
9H-5, 50-52	73.20	1.022	0.01	1.00	0.975	6.188	0.040	0.002
9H-5, 125-127	73.95	1.035	0.00	1.00	0.975	6.188	0.028	0.002
9H-6, 25-27	74.45	1.043	0.02	1.00	1.174	6.188	0.219	0.016
9H-6, 50-52	74.70	1.047	0.03	1.00	1.174	6.188	0.276	0.020
9H-6, 125-127	75.45	1.059	0.03	1.00	1.174	6.188	0.235	0.017
9H-7, 15-17	75.85	1.065	0.01	1.00	1.174	6.188	0.048	0.003
10H-1, 30-32	76.50	1.075	0.06	1.00	1.277	6.424	0.638	0.052
10H-1, 126-128	77.46	1.090	0.00	1.00	1.277	6.424	0.035	0.003
10H-2, 50-52	78.20	1.102	0.02	1.00	1.277	6.188	0.226	0.018
10H-2, 125-127	78.95	1.114	0.01	1.00	1.277	6.424	0.073	0.006
10H-3, 50-52	79.70	1.125	0.01	1.00	0.984	6.424	0.093	0.006
10H-3, 125-127	80.45	1.137	0.01	0.50	0.984	6.424	0.056	0.004
10H-4, 50-52	81.20	1.149	0.04	1.00	0.984	6.424	0.488	0.031
10H-4, 125-127	81.95	1.160	0.05	1.00	0.984	6.424	0.449	0.028
10H-5, 50-52	82.70	1.172	0.02	1.00	1.299	6.424	0.114	0.009
10H-5, 126-128	83.46	1.184	0.01	1.00	1.299	6.424	0.052	0.004
10H-6, 40-42	84.10	1.194	0.00	1.00	1.299	6.424	0.022	0.002
10H-6, 115-117	84.85	1.205	0.09	1.00	1.299	6.424	0.640	0.053
11H-1, 38-39	86.08	1.225	0.00	1.00	1.253	6.424	0.029	0.002
11H-1, 50-52	86.20	1.226	0.06	1.00	1.253	6.424	0.594	0.048
11H-1, 125-127	86.95	1.238	0.12	1.00	1.253	6.424	0.855	0.069
11H-2, 50-52	87.70	1.250	0.00	1.00	1.253	6.424	0.002	0.000
11H-2, 125-127	88.45	1.261	0.00	1.00	1.253	6.424	0.007	0.001
11H-3, 50-52	89.20	1.273	0.00	1.00	1.254	6.424	0.003	0.000
11H-3, 125-127	89.95	1.285	0.01	1.00	1.254	6.424	0.071	0.006
11H-4, 48-50	90.68	1.296	0.13	0.90	1.254	6.424	0.775	0.062
11H-4, 125-127	91.45	1.308	0.08	1.00	1.254	6.424	0.811	0.065
11H-5, 52-54	92.22	1.320	0.09	1.00	1.221	6.424	0.685	0.054
11H-5, 128-130	92.98	1.332	0.02	1.00	1.221	6.424	0.123	0.010
11H-6, 50-52	93.70	1.343	0.02	1.00	1.221	6.424	0.189	0.015
12H-1, 50-52	95.70	1.374	0.00	1.00	1.062	6.424	0.031	0.002
12H-1, 125-127	96.45	1.386	0.01	1.00	1.062	6.424	0.088	0.006
12H-2, 125-127	97.95	1.409	0.16	1.00	1.062	6.424	1.346	0.092
12H-3, 50-52	98.70	1.421	0.01	1.00	1.028	6.424	0.063	0.004
12H-3, 125-127	99.45	1.433	0.01	1.00	1.028	6.424	0.138	0.009
12H-4, 50-52	99.83	1.439	0.03	1.00	1.028	6.424	0.282	0.019
12H-4, 125-127	100.95	1.456	0.00	1.00	1.028	6.424	0.008	0.000
12H-5, 50-52	101.70	1.468	0.10	1.00	1.136	6.424	0.689	0.050
12H-5, 125-127	102.45	1.479	0.00	1.00	1.136	6.424	0.013	0.001
12H-6, 50-52	103.20	1.491	0.03	1.00	1.136	6.424	0.309	0.023
12H-6, 125-127	103.95	1.503	0.00	1.00	1.136	6.424	0.002	0.000
12H-7, 24-26	104.44	1.510	0.00	1.00	1.136	6.424	0.038	0.003
13H-1, 48-50	105.18	1.522	0.09	1.00	1.318	6.424	0.703	0.059
13H-1, 125-127	105.95	1.534	0.01	1.00	1.318	6.424	0.088	0.007

Appendix (continued).

Core, section, interval (cm)	Depth (mbsf)	Calculated age (Ma)	Coarse sand weight (g)	IRD (volumetric ratio)	Dry bulk density (g/cm^3)	Linear sedimentation rate (cm/k.y.)	IRD (wt%)	IRD MAR (g/cm^2/k.y.)
13H-2, 49-51	106.69	1.545	0.00	1.00	1.318	6.424	0.008	0.001
13H-2, 124-126	107.44	1.557	0.00	1.00	1.318	6.424	0.031	0.003
13H-2, 140-142	107.60	1.560	0.08	1.00	1.318	6.424	0.508	0.043
13H-3, 50-52	108.20	1.569	0.06	1.00	1.012	6.424	0.405	0.026
13H-3, 124-126	108.94	1.580	0.00	1.00	1.012	6.424	0.017	0.001
13H-4, 125-127	110.45	1.604	0.08	1.00	1.012	6.424	0.712	0.046
13H-4, 49-51	110.80	1.609	0.02	1.00	1.012	6.424	0.102	0.007
13H-5, 50-52	111.20	1.616	0.09	1.00	1.186	6.424	0.687	0.052
13H-5, 50-52	111.20	1.616	0.09	1.00	1.186	6.424	0.687	0.052
13H-5, 80-82	111.50	1.620	0.16	1.00	1.186	6.424	0.931	0.071
13H-5, 125-127	111.95	1.627	0.30	1.00	1.186	6.424	2.011	0.153
13H-6, 20-22	112.40	1.634	0.00	1.00	1.186	6.424	0.040	0.003
13H-6, 70-72	112.90	1.642	0.04	1.00	1.186	6.424	0.226	0.017
13H-7, 29-31	113.49	1.651	0.01	1.00	1.186	6.424	0.058	0.004
14H-1, 48-50	114.68	1.670	0.02	1.00	1.186	6.424	0.265	0.020
14H-1, 125-127	115.45	1.682	0.02	1.00	1.186	6.424	0.202	0.015
14H-2, 30-32	116.00	1.690	0.04	1.00	1.549	6.424	0.367	0.036
14H-2, 50-52	116.20	1.693	0.13	1.00	1.549	6.424	0.914	0.091
14H-2, 125-127	116.95	1.705	0.02	1.00	1.549	6.424	0.136	0.014
14H-3, 50-52	117.70	1.717	0.01	1.00	1.549	6.424	0.049	0.005
14H-3, 94-96	118.14	1.724	0.25	1.00	1.549	6.424	1.390	0.138
14H-3, 125-127	118.45	1.728	0.00	1.00	1.549	6.424	0.038	0.004
14H-4, 50-52	119.20	1.740	0.12	1.00	1.348	6.424	0.861	0.075
14H-4,125-127	119.95	1.752	0.00	1.00	1.348	6.424	0.034	0.003
14H-5, 50-52	120.70	1.763	0.01	1.00	1.348	6.424	0.040	0.003
14H-5, 125-127	121.45	1.780	0.12	1.00	1.348	3.25	0.930	0.041
14H-6, 50-52	122.20	1.787	0.05	1.00	1.356	6.424	0.302	0.026
14H-6, 125-127	122.95	1.799	0.01	1.00	1.356	3.25	0.044	0.002
14H-7, 16-18	123.36	1.805	0.11	1.00	1.356	3.25	0.621	0.027
14H-7, 40-42	123.60	1.809	0.13	1.00	1.356	3.25	0.924	0.041
14H-CC, 15-17	123.91	1.813	0.04	1.00	1.356	3.25	0.293	0.013
15H-1, 50-52	124.20	1.818	0.05	1.00	1.011	3.25	0.473	0.016
15H-1, 125-127	124.95	1.830	0.01	1.00	1.356	3.25	0.081	0.004
15H-2, 50-52	125.70	1.841	0.00	1.00	1.011	3.25	0.028	0.001
15H-2, 125-127	126.67	1.856	0.01	1.00	1.356	3.25	0.104	0.005
15H-3, 50-52	127.20	1.864	0.00	1.00	1.114	6.181	0.017	0.001
15H-3, 125-127	128.70	1.888	0.08	1.00	1.011	3.25	0.766	0.025
15H-5, 50-52	128.83	1.890	0.21	1.00	1.063	6.181	2.934	0.193
15H-5, 125-127	129.58	1.902	0.03	1.00	1.114	6.181	0.291	0.020
15H-6, 50-52	130.27	1.913	0.17	1.00	1.063	6.181	1.094	0.072
15H-6, 125-127	131.02	1.925	0.16	1.00	1.063	6.181	1.007	0.066
15H-7, 50-52	131.77	1.937	0.00	1.00	1.332	6.181	0.004	0.000
15H-7, 125-127	132.52	1.950	0.54	1.00	1.063	6.181	1.817	0.119
15H-8, 38-40	133.15	1.960	0.01	1.00	1.332	6.181	0.049	0.004
16H-1, 50-52	133.70	1.969	0.08	1.00	1.332	6.181	0.660	0.054
16H-1, 125-127	134.45	1.981	0.01	1.00	1.332	6.181	0.082	0.007
16H-2, 125-127	135.95	2.005	0.02	1.00	1.036	6.181	0.121	0.008
16H-3, 50-52	137.70	2.033	0.09	0.10	1.325	6.181	0.068	0.006
16H-4, 50-52	137.70	2.033	0.01	1.00	1.325	6.181	0.078	0.006
16H-5, 50-52	138.30	2.043	0.01	1.00	1.265	6.181	0.085	0.007
16H-6, 50-52	138.89	2.053	0.00	1.00	1.265	6.181	0.036	0.003
16H-7, 50-52	140.39	2.077	0.02	1.00	1.265	6.181	0.128	0.010
17X-1, 49-51	143.19	2.122	0.01	1.00	1.265	6.181	0.066	0.005
17X-1, 125-127	143.95	2.135	0.02	1.00	1.265	6.181	0.233	0.018
17X-2, 49-51	144.69	2.147	0.01	1.00	1.265	6.181	0.060	0.005
17X-2, 125-127	145.45	2.159	0.11	1.00	1.265	6.181	1.004	0.078
17X-3, 47-49	146.17	2.170	0.05	1.00	1.248	6.181	0.520	0.040
17X-3, 125-127	146.95	2.183	0.01	1.00	1.248	6.181	0.136	0.010
17X-4, 49-51	147.69	2.195	0.01	1.00	1.248	6.181	0.044	0.003
17X-4, 124-126	148.11	2.202	0.00	1.00	1.248	6.181	0.029	0.002
17X-5, 49-51	149.19	2.219	0.03	1.00	1.148	6.181	0.229	0.016
17X-5, 125-127	149.95	2.232	0.00	1.00	1.148	6.181	0.015	0.001
17X-6, 49-51	150.69	2.244	0.02	1.00	1.148	6.181	0.132	0.009
18X-1, 50-52	151.00	2.249	0.04	1.00	1.148	6.181	0.399	0.028
17X-6, 125-127	151.45	2.256	0.06	1.00	1.148	6.181	0.528	0.037
18X-1, 125-127	151.75	2.261	0.01	1.00	1.148	6.181	0.049	0.003
17X-7, 39-41	152.09	2.266	0.03	1.00	1.148	6.181	0.288	0.020

Appendix (continued).

Core, section, interval (cm)	Depth (mbsf)	Calculated age (Ma)	Coarse sand weight (g)	IRD (volumetric ratio)	Dry bulk density (g/cm^3)	Linear sedimentation rate (cm/k.y.)	IRD (wt%)	IRD MAR (g/cm^2/k.y.)
18H-2, 50-52	152.50	2.273	0.02	1.00	1.202	6.181	0.202	0.015
18X-2, 125-127	153.25	2.285	0.01	1.00	1.202	6.181	0.065	0.005
18X-3, 50-52	154.00	2.297	0.02	1.00	1.202	6.181	0.261	0.019
18X-3, 125-127	154.75	2.309	0.04	1.00	1.202	6.181	0.474	0.035
18X-4, 50-52	155.50	2.321	0.01	1.00	1.24	6.181	0.207	0.016
18X-4, 125-127	156.25	2.334	0.01	1.00	1.24	6.181	0.074	0.006
18X-5, 50-52	157.00	2.346	0.04	1.00	1.24	6.181	0.401	0.031
18X-5, 125-127	157.75	2.358	0.00	1.00	1.24	6.181	0.027	0.002
18X-6, 50-52	158.50	2.370	0.14	1.00	1.172	6.181	1.431	0.104
18X-6, 125-127	159.25	2.382	0.01	1.00	1.172	6.181	0.105	0.008
18X-7, 33-35	159.83	2.391	0.05	1.00	1.172	6.181	0.455	0.033
19X-1, 48-50	160.58	2.404	0.07	1.00	1.239	6.181	0.884	0.068
19X-1, 125-127	161.35	2.416	0.00	1.00	1.239	6.181	0.041	0.003
19X-2, 49-51	162.09	2.428	0.04	1.00	1.239	6.181	0.335	0.026
19X-2, 124-126	162.84	2.440	0.01	1.00	1.239	6.181	0.045	0.003
19X-3, 49-51	163.59	2.452	0.01	1.00	1.071	6.181	0.053	0.003
19X-3, 124-126	164.34	2.464	0.01	1.00	1.071	6.181	0.083	0.006
19X-4, 124-126	165.84	2.489	0.02	1.00	1.071	9.46	0.149	0.015
19X-5, 39-41	166.49	2.495	0.06	1.00	1.071	9.46	0.584	0.059
20X-1, 49-51	170.19	2.535	0.01	1.00	1.231	9.46	0.102	0.012
20X-1, 125-127	170.95	2.543	0.00	1.00	1.231	9.46	0.036	0.004
20X-2, 50-52	171.70	2.550	0.05	1.00	1.231	9.46	0.274	0.032
20X-2, 125-127	172.45	2.558	0.08	1.00	1.231	9.46	0.779	0.091
20X-3, 50-52	173.20	2.566	0.04	1.00	1.186	9.46	0.447	0.050
20X-3, 125-127	173.95	2.574	0.01	1.00	1.186	9.46	0.066	0.007
20X-4, 40-42	174.60	2.581	0.03	1.00	1.186	9.46	0.302	0.034
20X-4, 50-52	174.70	2.582	0.19	1.00	1.186	9.46	0.624	0.070
20X-4, 125-127	175.45	2.590	0.02	1.00	1.186	9.46	0.200	0.022
20X-5, 50-52	176.20	2.598	0.01	1.00	1.167	9.46	0.147	0.016
20X-5, 125-127	176.95	2.606	0.01	1.00	1.167	9.46	0.077	0.009
20X-6, 50-52	177.70	2.614	0.00	1.00	1.167	9.46	0.040	0.004
20X-6, 125-127	178.45	2.622	0.00	1.00	1.167	9.46	0.035	0.004
20X-7, 25-27	178.95	2.627	0.09	1.00	1.167	9.46	0.660	0.073
20X-CC, 25-27	179.27	2.630	0.01	1.00	1.167	9.46	0.125	0.014
21X-1, 49-51	179.79	2.636	0.03	1.00	1.009	9.46	0.241	0.023
21X-1, 125-127	180.55	2.644	0.01	1.00	1.009	9.46	0.038	0.004
21X-2, 50-51	181.30	2.652	0.04	1.00	1.009	9.46	0.292	0.028
21X-2, 125-127	182.05	2.660	0.01	1.00	1.009	9.46	0.054	0.005
21X-3, 49-51	182.79	2.668	0.08	1.00	1.007	9.46	0.564	0.054
21X-3, 125-127	183.55	2.676	0.01	1.00	1.007	9.46	0.046	0.004
21X-4, 21-23	184.01	2.681	0.09	1.00	1.007	9.46	0.767	0.073
21X-4, 49-51	184.29	2.684	0.01	1.00	1.007	9.46	0.066	0.006
21X-4, 125-127	185.05	2.692	0.01	1.00	1.007	9.46	0.069	0.007
21X-5, 49-51	185.79	2.699	0.01	1.00	1.032	9.46	0.039	0.004
21X-5, 125-127	186.55	2.707	0.02	1.00	1.032	9.46	0.168	0.016
21X-6, 49-51	187.29	2.715	0.22	1.00	1.032	9.46	1.611	0.157
21X-6, 87-89	187.67	2.719	0.23	1.00	1.032	9.46	1.907	0.186
21X-6, 125-127	188.05	2.723	0.06	1.00	1.032	9.46	0.491	0.048
21X-7, 19-21	188.49	2.728	0.00	1.00	1.032	9.46	0.029	0.003
22X-1, 49-51	189.39	2.737	0.02	1.00	1.159	9.46	0.196	0.021
22X-1, 127-129	190.17	2.746	0.02	1.00	1.159	9.46	0.199	0.022
22X-2, 51-53	190.91	2.754	0.01	1.00	1.159	9.46	0.095	0.010
22X-2, 127-129	191.67	2.762	0.10	1.00	1.159	9.46	0.971	0.106
22X-3, 49-51	192.39	2.769	0.00	1.00	1.01	9.46	0.008	0.001
22X-3, 125-127	193.15	2.777	0.07	1.00	1.01	9.46	0.655	0.063
22X-4, 50-52	193.90	2.785	0.01	1.00	1.01	9.46	0.083	0.008
22X-4, 123-125	194.63	2.793	0.03	1.00	1.01	9.46	0.398	0.038
22X-5, 46-48	195.36	2.801	0.03	0.80	1.017	9.46	0.373	0.036
22X-5, 83-85	195.73	2.804	0.34	1.00	1.017	9.46	3.662	0.352
22X-5, 127-129	196.17	2.809	0.00	1.00	1.017	9.46	0.043	0.004
22X-6, 48-50	196.88	2.817	0.06	1.00	1.017	9.46	0.489	0.047
22X-6, 125-127	197.65	2.825	0.03	1.00	1.017	9.46	0.232	0.022
22X-7, 29-31	198.19	2.830	0.08	1.00	1.017	9.46	0.497	0.048
23X-1, 50-52	199.00	2.839	0.00	1.00	1.093	9.46	0.044	0.005
23X-1, 125-127	199.75	2.847	0.00	1.00	1.093	9.46	0.002	0.000
23X-2, 50-52	200.50	2.855	0.01	1.00	1.093	9.46	0.039	0.004
23X-2, 125-127	201.25	2.863	0.01	1.00	1.093	9.46	0.043	0.004

Appendix (continued).

Core, section, interval (cm)	Depth (mbsf)	Calculated age (Ma)	Coarse sand weight (g)	IRD (volumetric ratio)	Dry bulk density (g/cm^3)	Linear sedimentation rate (cm/k.y.)	IRD (wt%)	IRD MAR ($g/cm^2/k.y.$)
23X-3, 50-52	202.00	2.871	0.27	1.00	1.466	9.46	2.180	0.302
23X-3, 125-127	202.75	2.879	0.01	1.00	1.466	9.46	0.039	0.005
23X-4, 50-52	203.50	2.887	0.01	1.00	1.466	9.46	0.076	0.010
23X-4, 125-127	204.25	2.895	0.13	1.00	1.466	9.46	1.047	0.145
23X-5, 50-52	205.00	2.902	0.06	1.00	1.066	9.46	0.519	0.052
23X-5, 125-127	205.75	2.910	0.06	0.90	1.066	9.46	0.421	0.042
23X-6, 50-52	206.50	2.918	0.01	1.00	1.066	9.46	0.101	0.010
23X-6, 125-127	207.25	2.926	0.01	1.00	1.066	9.46	0.066	0.007
24X-1, 46-48	208.56	2.940	0.00	1.00	1.087	9.46	0.014	0.001
24X-1, 126-128	209.36	2.949	0.16	0.95	1.087	9.46	1.203	0.124
24X-2, 53-55	210.13	2.957	0.02	1.00	1.087	9.46	0.359	0.037
24X-2, 124-126	210.84	2.964	0.10	0.90	1.087	9.46	1.005	0.103
24X-3, 49-51	211.59	2.972	0.00	1.00	0.921	9.46	0.047	0.004
24X-3, 129-131	212.39	2.981	0.00	1.00	0.921	9.46	0.028	0.002
24X-4, 47-49	213.07	2.988	0.03	1.00	0.921	9.46	0.307	0.027
24X-4, 124-126	213.84	2.996	0.01	1.00	0.921	9.46	0.051	0.004
24X-5, 50-52	214.60	3.004	0.01	1.00	0.997	9.46	0.111	0.010
24X-5, 124-126	215.34	3.012	0.00	1.00	0.997	9.46	0.059	0.006
24X-6, 48-51	216.08	3.020	0.00	1.00	0.997	9.46	0.021	0.002
24X-7, 19-21	217.29	3.032	0.00	1.00	0.997	9.46	0.034	0.003
24X-7, 61-63	217.71	3.037	0.02	1.00	0.997	9.46	0.219	0.021

Figure F1. Location map of Site 1101 on Drift 4 on the continental rise (after Rebesco et al., 1998).

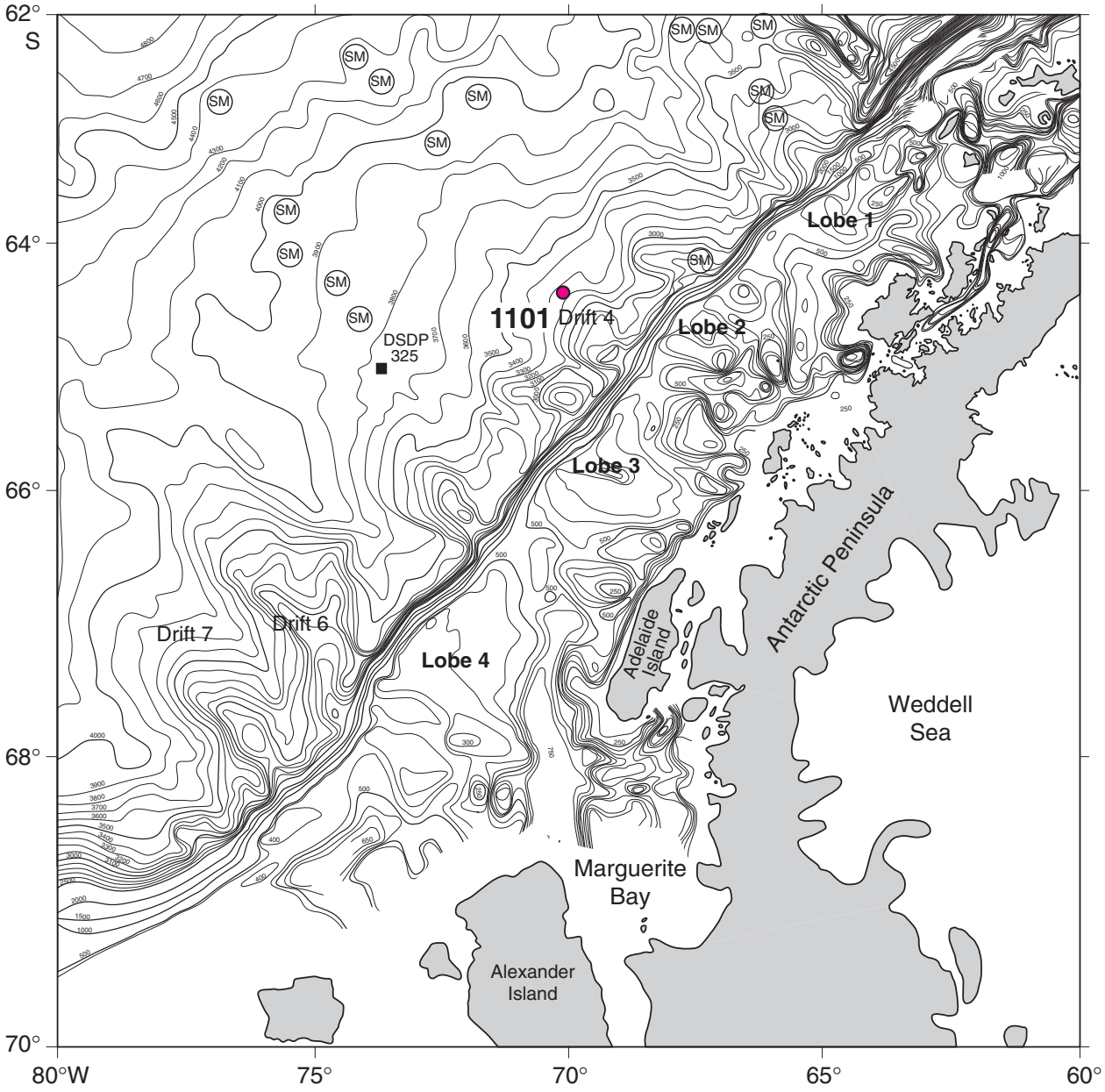

Figure F2. A. Abundance of coarse sand-sized (250 µm–2 mm) IRD as a function of depth. **B.** Mass accumulation rate of coarse sand-sized IRD as a function of age.

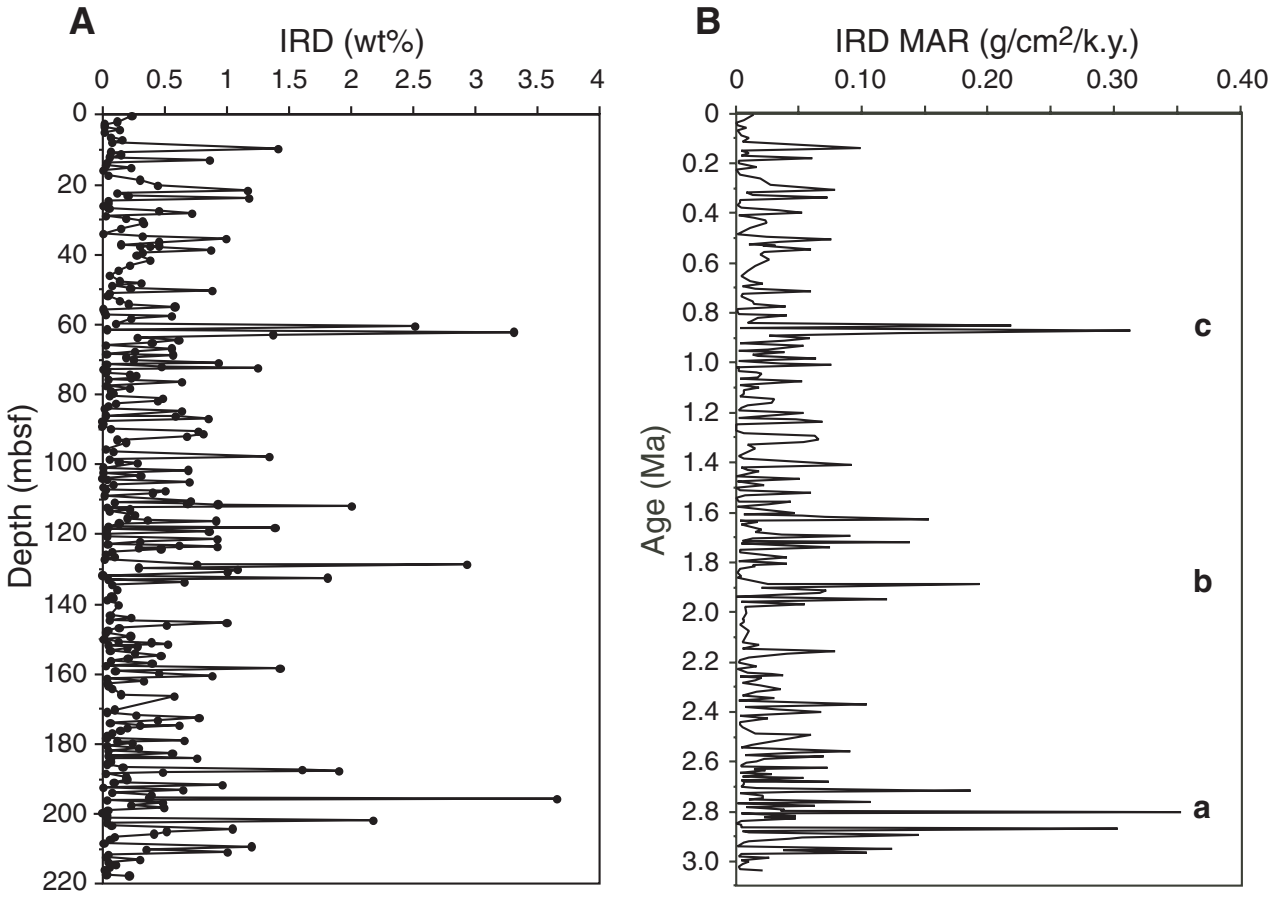

Figure F3. Lithofacies description of Sections 178-1101A-6H-1 to 11H-7, 38–95 mbsf, at Site 1101 with paleomagnetic polarity (black = normal, white = reversed) (from Barker, Camerlenghi, Acton, et al., 1999), extent of bioturbation, MS, IRD MAR, and number of clasts >2 mm. (This figure is also available in an **oversized format.**)

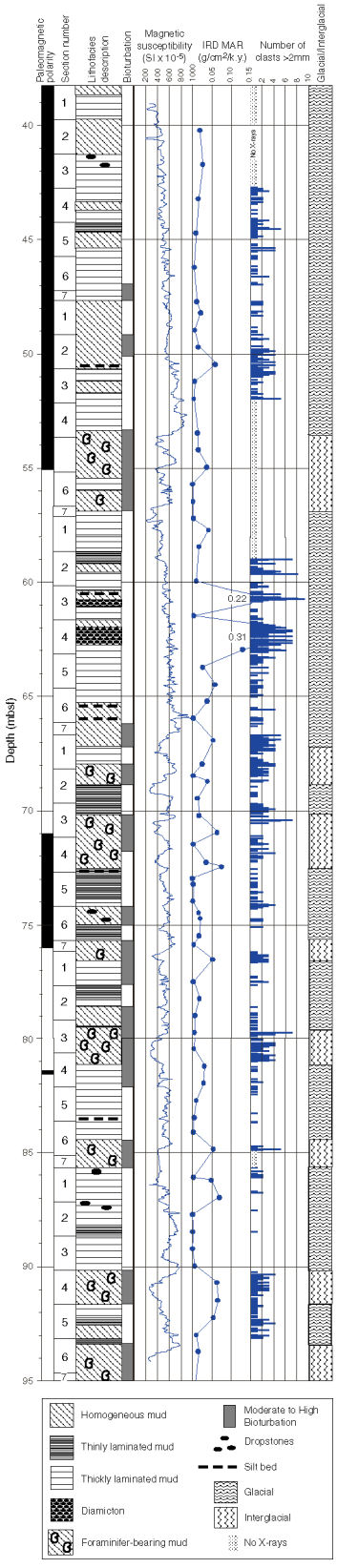

Figure F4. X-radiographs showing examples of laminated mud. Darker bands are silts, and low-density layers are more clay rich. **A.** Thickly laminated mud (interval 178-1101A-10H-6, 49–63 cm). **B.** Thickly laminated mud (interval 178-1101A-8H-3, 91–105 cm). Note the normal fault and isolated small pebbles. **C.** Thinly laminated mud (interval 178-1101A-10H-2, 10–24 cm). Some laminae are wavy and lenticular and others are planar.

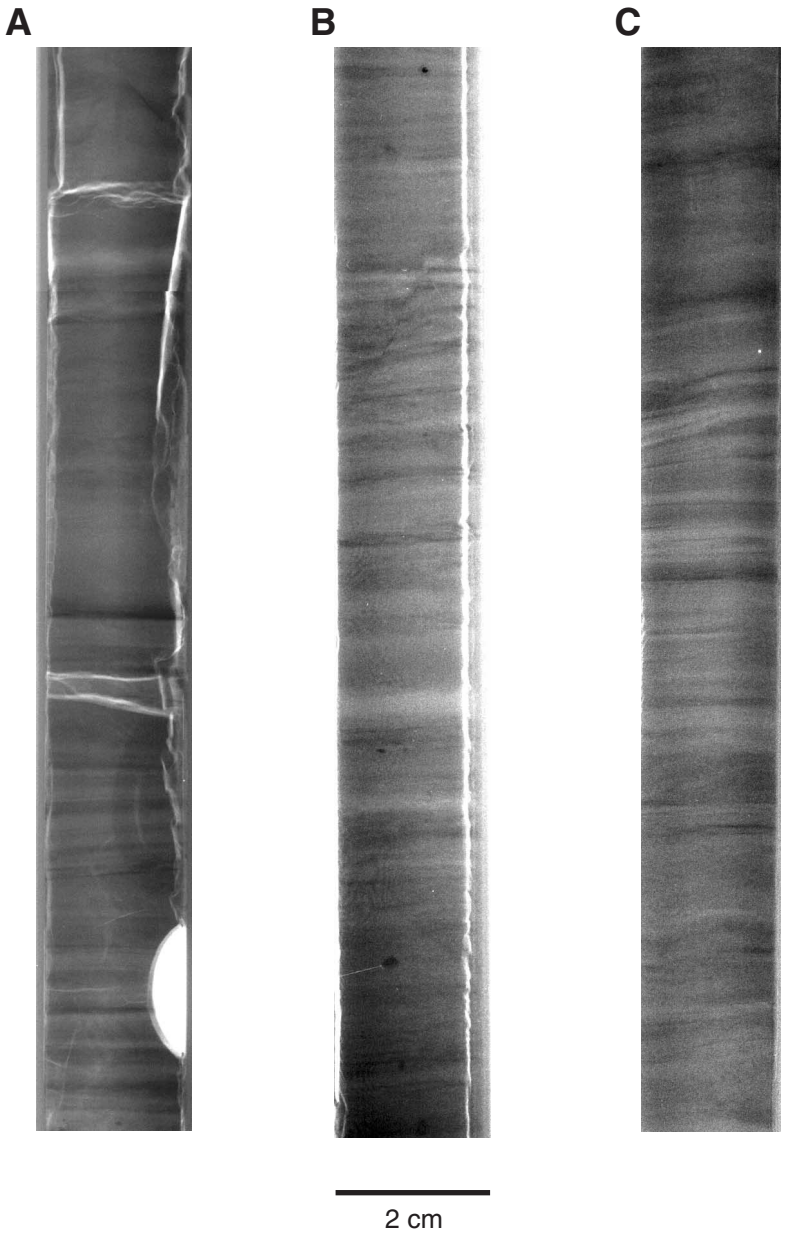

Figure F5. X-radiographs showing homogeneous mud, diamicton, and foraminifer-bearing mud. **A.** Homogeneous mud with an isolated dropstone (interval 178-1101A-8H-2, 54–68 cm). **B.** Homogeneous mud with scattered IRD. Low-density areas maybe caused by burrowing. **C.** Stratified diamicton produced by iceberg rafting (interval 178-1101A-8H-3, 54–68 cm). **D.** Foraminifer-bearing mud (interval 178-1101A-10H-5, 48–63 cm). The medium-density mottled appearance results from bioturbation.

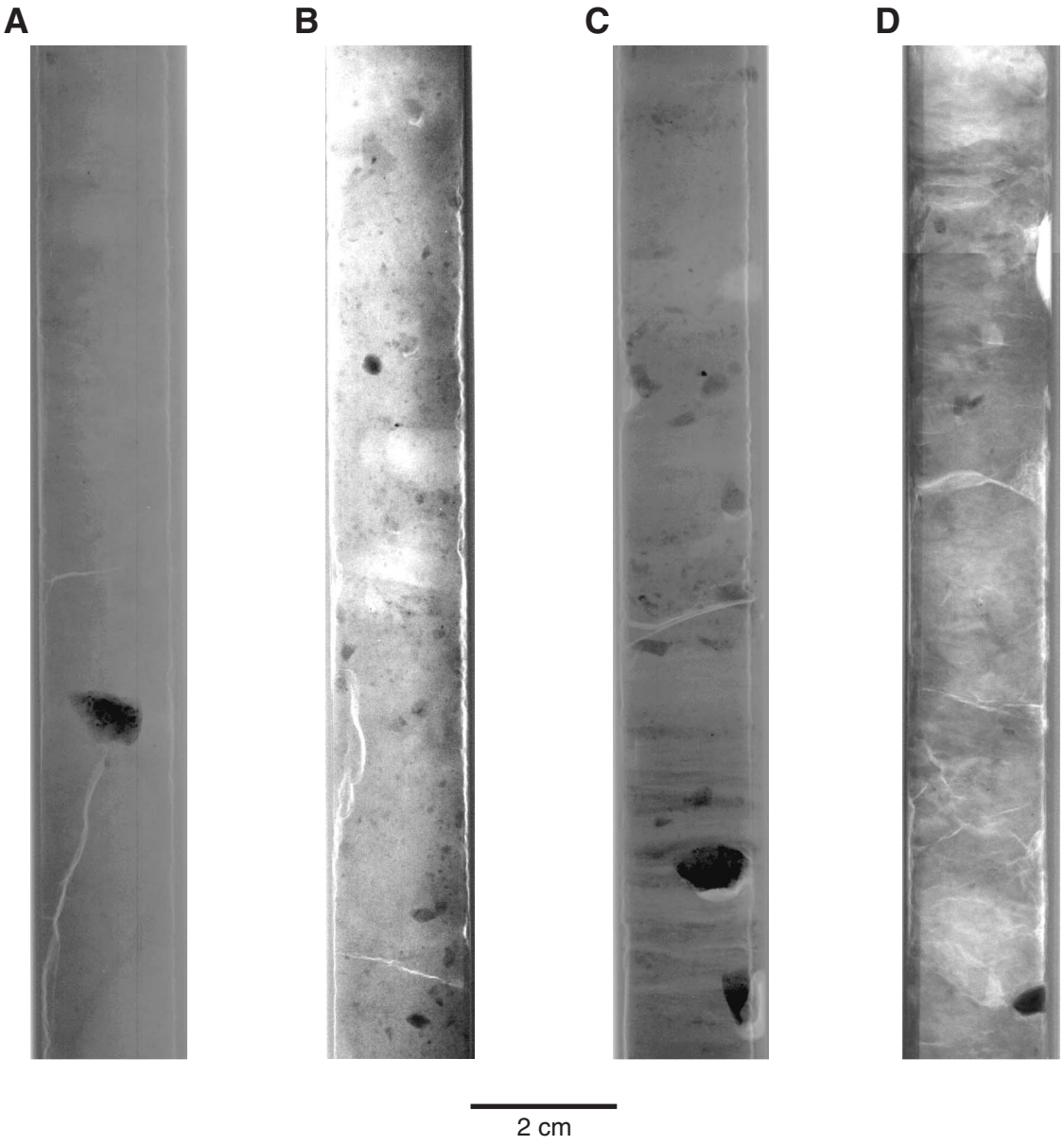

Table T1. Summary of depth ranges sampled, sample spacing, linear sedimentation rates, and resultant temporal spacing interval, Site 1101.

Depth (mbsf)	Sample spacing (cm)	Sedimentation rate (cm/k.y.)	Temporal sample spacing (k.y.)
0–55.08	75	7.06	10.6
55.08–71.2	75	7.68	9.8
71.2–76.15	75	6.19	12.1
76.15–121.12	75	6.42	11.7
121.12–126.98	75	3.25	23.1
126.98–165.98	75	6.18	12.1
165.98–209.4	75	9.46	7.9